Form-function relationship between trabecular bone architecture and biomechanical function in the horse humerus

Nicolas Cadoret, Chaves-Jacob Julien, Jean-Marc Linares, Alexandra Houssaye

Available online at www.sciencedirect.com

ScienceDirect

Procedia CIRP 110 (2022) 301–306

www.elsevier.com/locate/procedia

V CIRP Conference on Biomanufacturing

Form-function relationship between trabecular bone architecture and biomechanical function in the horse humerus

CADORET Nicolas[a], CHAVES-JACOB Julien[a,*], LINARES Jean-Marc[a], HOUSSAYE Alexandra[b]

[a] *Aix Marseille Université, CNRS, ISM, Inst Mouvement Sci, UMR 7287, Marseille, France*
[b] *Département Adaptations du Vivant, UMR 7179, CNRS/Muséum National d'Histoire Naturelle, 57 rue Cuvier, CP-55, Paris, 75005, France*

* Corresponding author. *E-mail address:* julien.CHAVES-JACOB@univ-amu.fr

Abstract

In mechanical design, it is a common challenge to design parts with high strength-to-weight ratio. Throughout evolution, natural organisms have faced the same challenge and developed a variety of solutions. One of these is the endoskeleton, composed of bones linked by joints. In long bones, near joints, Nature uses an anisotropic porous material, trabecular bone. This architecture is adapted to the mechanical stresses it undergoes. The aim of this work is to study the relationship between a given trabecular architecture and its biomechanical function. Understanding this relationship allows to predict the natural trabecular architecture that would be optimal to support a given stress field. Trabecular architecture is often characterised through a Fabric Tensor (FT) whose eigenvectors and eigenvalues respectively describe trabecular orientation and anisotropy. A first FT ($\boldsymbol{M_{mes}}$) was measured using BoneJ2 in 20 trabecular Regions Of Interest (ROI) identified in a microtomographied horse humerus. In parallel, the stress field in this humerus was calculated using a Finite Elements Analysis (FEA) based on a musculoskeletal model of the horse forelimb during trotting. This FEA was used to obtain a second FT ($\boldsymbol{M_{est}}$) for each ROI through an equation from the literature relating FT to stress in the human femur. Difference percentages between $\boldsymbol{M_{mes}}$ and $\boldsymbol{M_{est}}$ were calculated and showed that the proposed law is accurate to predict FT from stress in the horse humerus. This law is interesting for the design of mechanical parts bio-inspired from bones, which reproduce the adaptation of trabecular architecture to the mechanical stress it undergoes.

Keywords: Bio-inspiration; Bones; Trabecular Architecture; Stress Tensor; Fabric Tensor

1. Introduction

Throughout Evolution, natural organisms have developed an abundance of solutions as a result of evolutionary pressure and natural selection. These solutions respond to a wide variety of functions needed for an organism's survival. For an engineer, these solutions can be an endless source of inspiration in the context of technical challenges. Indeed, organisms are subjected to similar constraints as most mechanical designs: optimising the mass, ensuring no critical failure, limiting resource consumptions, etc. This design approach is known as biomimicry or bio-inspiration. It has seen increased interest in recent years because of two major factors. First, bio-inspiration can help develop innovative and sustainable engineering applications and solutions [1]. Second, bio-inspiration in mechanical design often results in complex geometries. The manufacturing of such geometries has recently become cost-effective thanks to the spread of Additive Manufacturing (AM) technologies. Indeed, AM decorrelates the manufacturing cost of mechanical parts from their complexity [2].

In the context of mechanical design, optimising a part's strength-to-weight ratio is a recurring challenge. Increasing the

2212-8271
10.1016/j.procir.2022.06.054

strength-to-weight ratio allows to reduce a part's mass whilst maintaining similar performances. Reduced mass leads to reduced energy consumption for the mechanical system. Increasing the strength-to-weight ratio can be done through techniques such as topology optimisation, lattice structures [3,4] or by selecting materials for their strength-to-weight ratio. In fact, natural cellular materials such as wood and bone are examples of materials with high strength-to-weight ratios [5] which have been used extensively throughout History. Wood and bone are defined as hierarchical materials [6,7] with complex architectures that can be inspiration sources for engineers.

Bones in particular fulfil key mechanical functions in endoskeletons which explain their architecture. Bones provide a frame upon which muscles attach. They keep the body supported, are involved in body segments' movements, provide leverage and transmit forces [8]. At the tissue level, bone differentiates into trabecular spongy bone and cortical compact bone. This differentiation, beyond a different initial deposit mode, is also a result of mechanically-driven functional adaptation of the bone tissue through bone remodelling [9,10]. Trabecular bone transfers load from articular areas toward cortical bone which provides most of the support. In fact Wolff's Law, established in 1870, states that bone has the ability to adapt to mechanical stimulus to reach an optimised architecture [11,12].

Bones' complex architecture can be studied through histomorphometry [13]. In particular, the Mean Intercept Length (MIL) based Fabric Tensor (FT) represents a trabecular architecture's orientation and degree of anisotropy [14,15]. An FT is defined as "a symmetric second rank tensor which characterises the arrangement of the microstructural components in a multiphase or porous material" [16]. For trabecular bone, FT and volume fraction can explain 98% of the variation in mechanical properties between anatomical sites [17]. Wolff's Law states that bone architecture (the tissue's arrangement) is a consequence of its mechanical environment (the tissue's biomechanical function). Thus, it is reasonable to expect that a mathematical link exists between stress and fabric tensors. Such a relationship has been proposed by Hazrati Marangalou et al. [18] in the case of the walking human femur.

Because animal skeletons have adapted differently to biomechanical stresses in different evolutionary lineages, the study of other animal models is of great interest to better characterise this trabecular form-function relationship. In the following work, the proposed relationship will be validated in the case of the trotting horse humerus. First, the stress field inside the horse humerus was simulated based on a musculoskeletal model of the trotting horse forelimb [19]. The resulting Finite Elements Analysis (FEA) helped identify 20 trabecular Regions Of Interest (ROI) in a horse humerus CT scan. Then, MIL-based FT was measured for these 20 ROIs. Finally, the measured MIL-based FT ($\boldsymbol{M_{mes}}$) was compared to the stress-estimated FT ($\boldsymbol{M_{est}}$) obtained through the aforementioned relationship [18]. Difference percentages between $\boldsymbol{M_{mes}}$ and $\boldsymbol{M_{est}}$ were computed to validate the proposed form-function relationship in the trotting horse humerus.

2. Materials & Methods

The first step to study the trabecular form-function relationship in the horse humerus is to estimate the stress field that the bone undergoes during typical physical activity, for example trotting.

2.1. Simulating stress field in the horse humerus during trotting

In order to estimate the stress field in the trotting horse humerus, a complete gait simulation of the horse forelimb is needed. This simulation is able to estimate articular and muscular loadings during the trotting gait. This work was first carried out to estimate contact pressures in the horse forelimb joints for bio-inspired design purposes [19]. The model and its outputs are described in details in Becker et al.'s work but will be described briefly below.

First, joints and segments of a French saddle horse's forelimb were identified with markers and tracked with a video camera during trotting and jumping. Ground reaction forces were measured through a buried force plate. Marker trajectories were traced with the Kinovea software. Bones, muscles, tendons and ligaments were reproduced from Biosphera into CATIA V5. Finally, a musculoskeletal kinetic model of the trotting and jumping horse forelimb was generated with OpenSim based on Kinovea trajectories and CATIA V5 geometries.

From this musculoskeletal model, articular and muscular forces supported by the horse humerus were estimated at 8 time steps of peak muscular activity during the trotting gait**.** Following this simulation of the trotting gait, a Finite Elements Analysis (FEA) of the trotting horse humerus was created.

8 static analysis of the horse humerus were created for the 8 identified peak muscular activity time steps. Internal and external bone geometry were obtained from a CT scan of a racing horse humerus performed at the AST-RX platform at the Museum National d'Histoire Naturelle, Paris (UMS 2700; GE phoenix|X-ray v|tome|xs 240), with reconstructions performed using X-Act (RX Solutions). The resolution of this CT scan is 1 voxel per 0.09 mm. Boundary conditions were applied to best reflect the biological reality with pressures applied to joints and tendon connective zones. The inertia relief method was applied to ensure static equilibrium of the humerus [20]. The FE mesh consists of second order tetrahedral elements with maximum sizes of 5mm on the surface and 2mm inside the humerus.

These 8 analysis configurations result in an overview of the stress field throughout the horse humerus during trotting. Based on these results, 20 ROIs were selected from the horse humerus CT scans' trabecular tissue in order to cover a wide range of tissue arrangement. Peak local stress (PLS) conditions for each ROI were identified amongst the 8 FEA configurations based on the maximal Von Mises stress criteria. The resulting ROI average stress tensor was then eigendecomposed into principal stress values and directions. This work focuses on principal stress values. It was hypothesised that traction and compression have similar effects on trabecular bone's functional adaptation [21]. Thus, in this work, principal stress values were sorted in

descending order of absolute value ($|\sigma_1| \geq |\sigma_2| \geq |\sigma_3|$). These results are given in section 3.1

2.2. Measuring Fabric Tensors in 20 regions of interest of the horse humerus

Section 2.1 allowed to identify 20 trabecular ROIs and their respective PLS conditions. This represents the maximal mechanical constraints a given bone region needs to overcome. To study the trabecular form-function relationship, we still need to describe the tissue arrangement in a given bone region. As stated previously, the MIL-based FT describes a trabecular sample's orientation and degree of anisotropy [22]. Hence, the 20 ROIs identified previously were segmented from the overall CT scan of the horse humerus. MIL-based FT was measured for each ROI through BoneJ2 anisotropy plug-in [23].

The FT outputted by the Anisotropy plug-in is presented as the principal radii ($c \geq b \geq a$), eigenvectors and Degree of Anisotropy (*DA*) of the ellipsoid fitted to the MIL points. For the purpose of this work, principal radii and *DA* were considered. MIL-based FT radii describe anisotropy of the considered trabecular sample in a direction. The measured MIL-based FT radii were normalised into ($M_{1_{mes}} \geq M_{2_{mes}} \geq M_{3_{mes}}$) through Eq.(1) in order to ensure that $\det(\boldsymbol{M_{mes}}) = 1$. These results are given in section 3.2.

$$\boldsymbol{M_{mes}} = \begin{bmatrix} M_{1_{mes}} & 0 & 0 \\ 0 & M_{2_{mes}} & 0 \\ 0 & 0 & M_{3_{mes}} \end{bmatrix} = k.\begin{bmatrix} c & 0 & 0 \\ 0 & b & 0 \\ 0 & 0 & a \end{bmatrix} \quad (1)$$

$$with\ k = \frac{1}{\sqrt[3]{a.b.c}}$$

2.3. Validity of a trabecular form-function relationship between Fabric Tensor and principal stress in the horse humerus

As stated in section 1, Hazrati Marangalou et al. [18] proposed a form-function relationship for the walking human femur Eq.(2). This relationship allows to estimate a trabecular sample's FT ($\boldsymbol{M_{est}}$) in light of the local stress conditions this sample undergoes. The validity of $\boldsymbol{M_{est}}$ was verified with regard to the data gathered for the horse humerus. In particular, percentage differences between measured MIL-based FT ($\boldsymbol{M_{mes}}$) and stress-estimated FT ($\boldsymbol{M_{est}}$) were computed.

$$M_{i_{est}} = \frac{|\sigma_i|^{1/4}}{(|\sigma_1|^{1/4}.|\sigma_2|^{1/4}.|\sigma_3|^{1/4})^{1/3}} \quad (2)$$

For every ROI, ($M_{1_{est}} \geq M_{2_{est}} \geq M_{3_{est}}$) were computed based on principal stress values ($|\sigma_1| \geq |\sigma_2| \geq |\sigma_3|$) for the PLS condition. Then, percentage differences were computed between ($M_{1_{mes}} \geq M_{2_{mes}} \geq M_{3_{mes}}$) and ($M_{1_{est}} \geq M_{2_{est}} \geq M_{3_{est}}$) to study the validity of Hazrati Marangalou et al. [18] relationship in the case of the trotting horse humerus. These results are given in section 3.3.

Table 1: principal stress values ($|\sigma_1| \geq |\sigma_2| \geq |\sigma_3|$), degree of anisotropy (*DA*) and normalised measured Mean Intercept Length based Fabric Tensor radii ($M_{1_{mes}} \geq M_{2_{mes}} \geq M_{3_{mes}}$) for peak local stress condition in 20 regions of interest of the trotting horse humerus.

	$\lvert\sigma_1\rvert$	$\lvert\sigma_2\rvert$	$\lvert\sigma_3\rvert$	*DA*	$\boldsymbol{M_{1_{mes}}}$	$\boldsymbol{M_{2_{mes}}}$	$\boldsymbol{M_{3_{mes}}}$
ROI1	5.972	3.315	0.238	0.514	1.243	0.929	0.866
ROI2	3.743	1.824	0.440	0.343	1.134	0.959	0.919
ROI3	5.039	1.761	0.078	0.384	1.156	0.954	0.907
ROI4	4.042	2.389	0.428	0.308	1.098	0.997	0.914
ROI5	2.524	0.880	0.778	0.433	1.160	0.987	0.874
ROI6	2.999	1.587	0.885	0.578	1.218	1.038	0.791
ROI7	4.207	1.483	1.027	0.403	1.140	0.995	0.881
ROI8	7.353	0.525	0.006	0.726	1.395	0.981	0.731
ROI9	2.407	1.945	0.426	0.374	1.143	0.967	0.904
ROI10	6.483	0.554	0.426	0.491	1.228	0.930	0.876
ROI11	6.356	3.976	1.872	0.137	1.042	0.991	0.968
ROI12	11.924	3.751	0.385	0.459	1.120	1.084	0.824
ROI13	7.453	1.192	0.579	0.368	1.142	0.964	0.908
ROI14	5.409	2.059	0.301	0.549	1.204	1.027	0.809
ROI15	18.552	5.622	0.801	0.783	1.445	1.027	0.673
ROI16	5.332	4.740	0.587	0.704	1.303	1.083	0.708
ROI17	10.035	3.260	0.122	0.646	1.369	0.896	0.815
ROI18	12.026	2.752	1.890	0.484	1.189	0.985	0.854
ROI19	9.967	5.002	0.399	0.636	1.231	1.095	0.742
ROI20	4.372	2.422	0.087	0.350	1.125	0.980	0.907

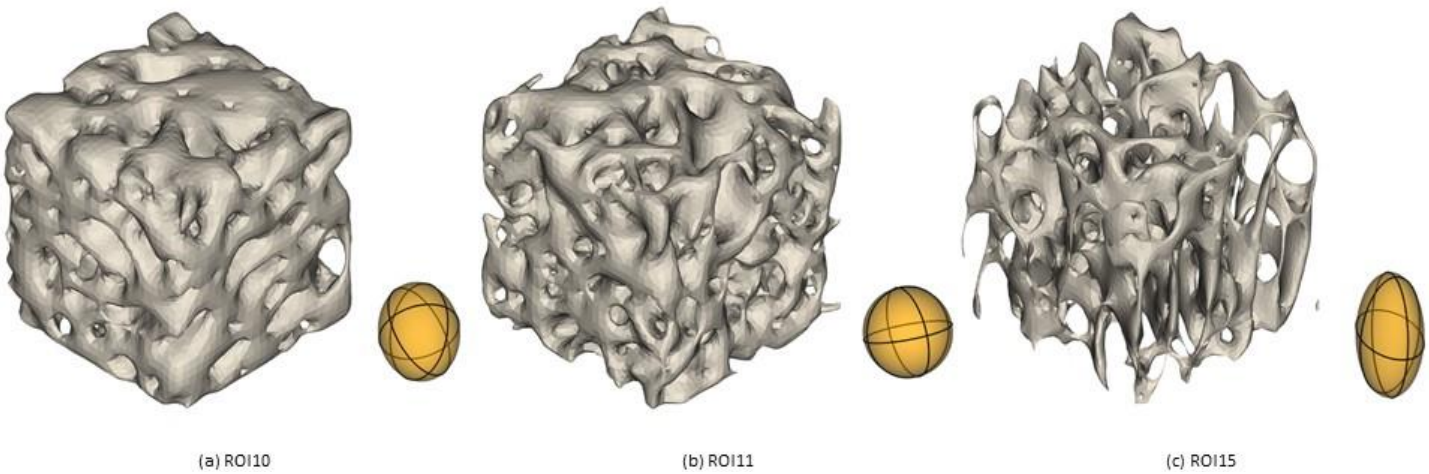

Fig. 1. representation of ROI10 (a), ROI11 (b) and ROI15 (c) and their respective Mean Intercept Length based Fabric Tensor ellipsoids after Laplacian smoothing of initial ROI STL.

3. Results

3.1. Stress field in the horse humerus during trotting

Principal stress values ($|\sigma_1| \geq |\sigma_2| \geq |\sigma_3|$) for the 20 ROIs during PLS conditions are reported in Table 1. All PLS conditions are grouped into the stance phase of the trotting gait.

3.2. Fabric Tensors of 20 trabecular regions of interest in the horse humerus

Table 1 shows *DA* and normalised MIL-based FT radii ($M_{1_{mes}} \geq M_{2_{mes}} \geq M_{3_{mes}}$) for the 20 ROIs. Amongst the 20 ROIs, three were chosen based on *DA* to represent the varying degrees of anisotropy that can be found in trabecular samples. *DA* can vary between 0 and 1. Thus, the most anisotropic ROI (maximal *DA*), the least anisotropic ROI (minimal *DA*) and a moderately anisotropic ROI (*DA* closest to 0.5) were selected. They were represented with their respective MIL-based FT ellipsoids in Fig. 1:

- ROI10; *DA* = 0.491, a moderately anisotropic ROI
- ROI11; *DA* = 0.137, the least anisotropic ROI
- ROI15; *DA* = 0.782, the most anisotropic ROI

This representation was created with FreeCAD Mesh Design and Part design workbenches [24]. Initial ROI STL exported from ImageJ were submitted to Laplacian smoothing to facilitate visualisation. MIL-based FT ellipsoids were generated based on BoneJ2's Anisotropy results. As is especially clear for ROI15 on Fig. 1(c), MIL-based FT ellipsoids follow the predominant trabecular orientation. Furthermore, the shape of the MIL-based FT ellipsoid is an indicator of a trabecular sample's anisotropy.

3.3. Trabecular form-function relationship through Fabric Tensor and principal stresses in the horse humerus

Percentage differences were computed through Eq.(3) between ($M_{1_{mes}} \geq M_{2_{mes}} \geq M_{3_{mes}}$) and ($M_{1_{est}} \geq M_{2_{est}} \geq M_{3_{est}}$). These results are given in Table 2.

$$E_i = \left| \frac{M_{i_{est}} - M_{i_{mes}}}{M_{i_{mes}}} \right| \quad (3)$$

Percentage differences given in Table 2 are also shown in Fig. 2 for each ROI. As showcased on this histogram, estimation of the MIL-based FT from PLS condition principal stress values produces an average of 15.64% differences with measured MIL-based FT. It should be noted that some ROIs contribute significantly more than others to the mean difference. For example, removing ROI8 from the dataset lowers the mean difference percentage to 14.21%. These mean difference percentages are on par with Hazrati Marangalou et al. [18] results who showed 9.21% mean averaged norm differences between actual and estimated FT for ten samples in the walking human femur.

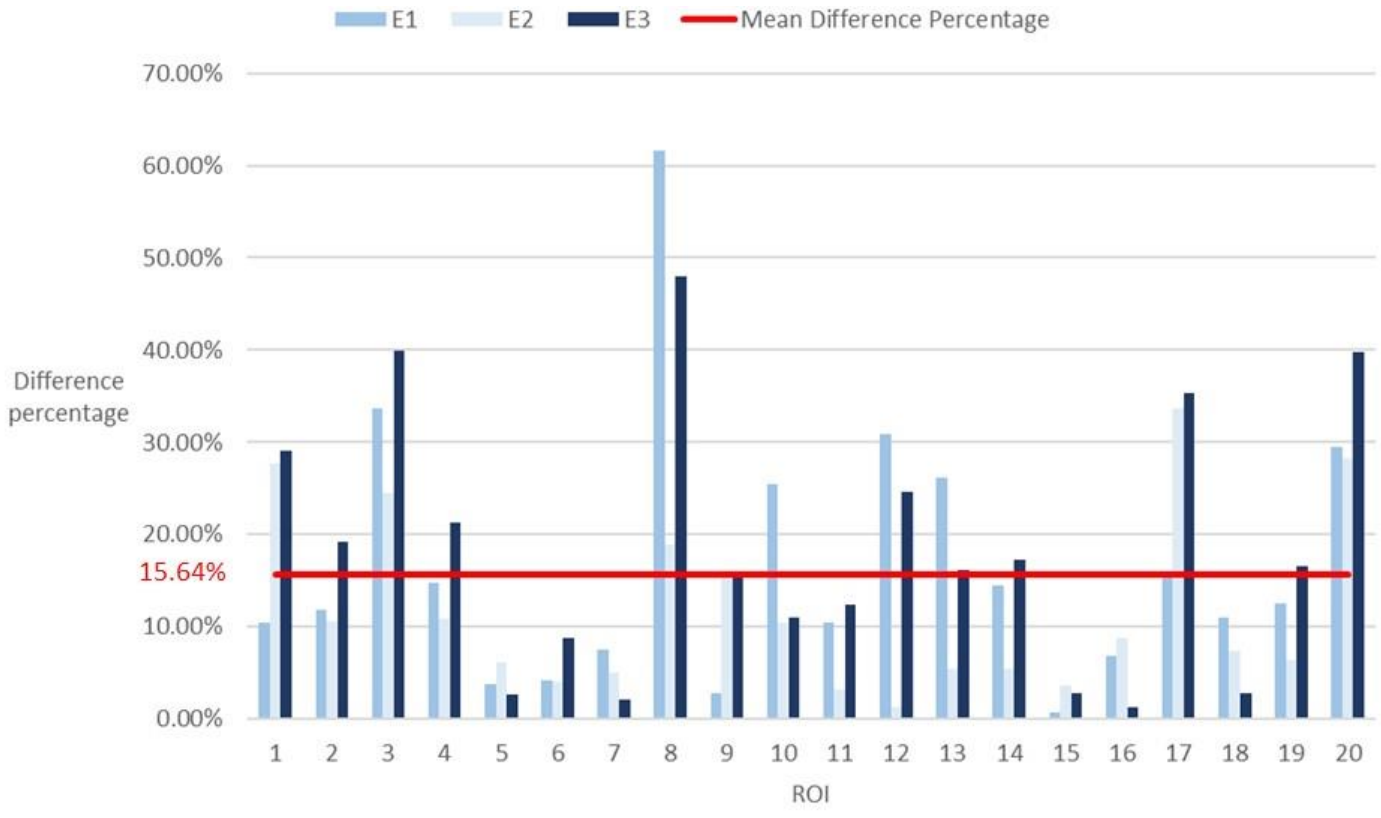

Fig. 2. percentage differences (E_1,E_2,E_3) between estimated (M_(1_est)≥M_(2_est)≥M_(3_est)) and measured (M_(1_mes)≥M_(2_mes)≥M_(3_mes)) Fabric Tensor radii for peak local stress condition in 20 regions of interest of the horse humerus

Table 2: Stress-estimated normalised Mean Intercept Length based Fabric Tensor radii ($M_{1_{est}} \geq M_{2_{est}} \geq M_{3_{est}}$) and percentage differences (E_1, E_2, E_3) between estimated and measured Fabric Tensor radii for peak local stress condition in 20 regions of interest of the horse humerus

	$M_{1_{est}}$	$M_{2_{est}}$	$M_{3_{est}}$	E_1	E_2	E_3
ROI1	1.374	1.186	0.614	10.52%	27.68%	29.13%
ROI2	1.269	1.060	0.743	11.90%	10.56%	19.17%
ROI3	1.545	1.188	0.545	33.63%	24.55%	39.92%
ROI4	1.260	1.105	0.719	14.72%	10.81%	21.34%
ROI5	1.204	0.925	0.897	3.83%	6.21%	2.69%
ROI6	1.167	0.996	0.860	4.17%	4.04%	8.74%
ROI7	1.227	0.945	0.862	7.58%	5.02%	2.14%
ROI8	2.256	1.166	0.380	61.65%	18.86%	47.95%
ROI9	1.176	1.115	0.763	2.84%	15.29%	15.66%
ROI10	1.540	0.833	0.780	25.47%	10.49%	10.96%
ROI11	1.151	1.024	0.848	10.49%	3.28%	12.37%
ROI12	1.466	1.098	0.621	30.95%	1.25%	24.58%
ROI13	1.441	0.912	0.761	26.19%	5.42%	16.21%
ROI14	1.379	1.083	0.670	14.50%	5.48%	17.20%
ROI15	1.435	1.065	0.654	0.71%	3.65%	2.83%
ROI16	1.214	1.179	0.699	6.85%	8.79%	1.32%
ROI17	1.586	1.197	0.527	15.79%	33.65%	35.38%
ROI18	1.319	0.913	0.831	10.96%	7.33%	2.75%
ROI19	1.385	1.166	0.619	12.55%	6.46%	16.54%
ROI20	1.457	1.257	0.546	29.46%	28.25%	39.77%

4. Discussion

Hence, through this work, a proposed trabecular form-function relationship for the walking human femur was validated in the context of the trotting horse humerus. This was done in light of estimated local stress for PLS conditions during the trotting gait and measured MIL-based FT for 20 ROIs of the horse humerus.

The mean difference percentage between $\boldsymbol{M_{mes}}$ and $\boldsymbol{M_{est}}$ for all 20 ROIs is 15.64% with a few ROIs contributing heavily to this mean difference percentage. It is possible that principal stress values in those ROIs are overestimated due to the conditions of the FEA. This would lead to an overestimated FT and significant difference percentages, such as the one observed for ROI8. It should also be noted that a more diverse phenomenon is involved in the functional adaptation of bone than the one considered in this study. Indeed, bone is a living tissue that takes part in complex homeostatic equilibrium. Regardless, the mean difference percentage is low enough to validate the use of the proposed relationship in the context of the trotting horse humerus.

The same type of study should be conducted to validate and adapt this relationship in other context than the walking human femur and the trotting horse humerus. Indeed, for bio-inspired mechanical design, establishing a generic law is important because it broadens the range of parts that can be designed through a specific approach. Given that animal skeletons have adapted differently to biomechanical stresses in different evolutionary lineages, a wide range of data sets could lead to a more broadly applicable bio-inspired design law. Hence, the study of other animal models is of great interest to better characterise the trabecular form-function relationship. For example, other mammalian bones and movement cycles could be studied. Samples could also be compared between the same bone region in different specimens, etc. The resulting law would be more easily applicable to mechanical design issues but less specific for biological cases.

It should be noted that Hazrati Marangalou et al. showed lower mean differences percentages between estimated and measured FT in the human femur. This is explained by the modelling approach which used iterative FEA to estimate an FT, with around 20 iterations needed to converge. In the present work, direct FEA results were used to estimate FT and resulted in slightly higher difference percentages. It is expected that accuracy could be improved through an iterative approach similar to Hazrati Marangalou et al.'s. Furthermore, only the trotting gait was considered to represent typical physical activity of the horse humerus. In reality, the horse humerus undergoes and is adapted to a wide variety of mechanical constraints such as landing from jumps, galloping, etc. It is expected that considering a wider range of physical activities, closer to the biological reality, could further improve FT prediction accuracy.

Throughout this work, the biomechanical stimuli considered for the trabecular form-function relationship is the principal stress values for PLS conditions. In light of the prediction capabilities of the proposed relationship for FT, this hypothesis seems reasonable. This could indicate that trabecular tissue has the ability to adapt to the relative maximal stress it undergoes over a given period of time. Put differently, PLS conditions principal stress could be the stimuli that dictates functional adaptation of the trabecular tissue.

In the context of mechanical design, better understanding the trabecular form function relationship can prove very useful. Indeed, if one is able to replicate this form-function relationship in an algorithmically-generated architecture, it should be possible to replicate bone's optimised strength-to-weight ratio. Applied to mechanical parts, this could lead to reduced mass with similar performance and reduced energy consumption for the mechanical system.

5. Conclusions

Throughout this work, the form-function relationship of trabecular bone was studied. In particular, a relationship proposed by Hazrati Marangalou et al. in the case of the walking human femur was validated in the case of the trotting horse humerus. The dataset used for that purpose was build by estimating the principal stress values under Peak Local Stress conditions during the trotting gait and measuring Mean Intercept Length based Fabric Tensors for 20 Regions of Interest selected in the horse humerus. This measured MIL-based FT was compared to a stress-estimated FT and low percentage differences were found.

Acknowledgements

We warmly thank Pauline Hanot (UMR 7179, MNHN, Paris, France) for the loan of the specimen needed for this work and M. Bellato (UMS 2700, MNHN, Paris, France) for performing the scan and reconstruction. This project has received financial support from the CNRS through the Mission for Transversal and Interdisciplinary Initiatives (MITI program).

References

[1] du Plessis A, Broeckhoven C, Yadroitsava I, Yadroitsev I, Hands CH, Kunju R, et al. Beautiful and Functional: A Review of Biomimetic Design in Additive Manufacturing. Additive Manufacturing 2019;27:408–27..

[2] Schmidt M, Merklein M, Bourell D, Dimitrov D, Hausotte T, Wegener K, et al. Laser based additive manufacturing in industry and academia. CIRP Annals 2017;66:561–83.

[3] Ding Y. Shape optimization of structures: a literature survey. Computers & Structures 1986;24:985–1004.

[4] Pan C, Han Y, Lu J. Design and Optimization of Lattice Structures: A Review. Applied Sciences 2020;10:6374.

[5] Gibson LJ. Biomechanics of cellular solids. Journal of Biomechanics 2005;38:377–99.

[6] Fratzl P, Weinkamer R. Nature's hierarchical materials. Progress in Materials Science 2007;52:1263–334..

[7] Reznikov N, Shahar R, Weiner S. Bone hierarchical structure in three dimensions. Acta Biomaterialia 2014;10:3815–26.

[8] Houssaye A, Taverne M, Cornette R. 3D quantitative comparative analysis of long bone diaphysis variations in microanatomy and cross-sectional geometry. Journal of Anatomy 2018;232:836–49.

[9] Frost HM. Bone mass and the mechanostat: A proposal. Anat Rec 1987;219:1–9.

[10] Frost HM. Bone's mechanostat: A 2003 update. Anat Rec 2003;275A:1081–101..

[11] Willie B, Duda GN, Weinkamer R. CHAPTER 2. Bone Structural Adaptation and Wolff's Law. In: Fratzl P, Dunlop JWC, Weinkamer R, editors. Materials Design Inspired by Nature: Function Through Inner Architecture, Cambridge: Royal Society of Chemistry; 2013, p. 17–45.

[12] Wolff J. The Classic: On the Inner Architecture of Bones and its Importance for Bone Growth: (Ueber die innere Architectur der Knochen und ihre Bedeutung für die Frage vom Knochenwachsthum). Clinical Orthopaedics and Related Research® 2010;468:1056–65.

[13] Parfitt AM, Drezner MK, Glorieux FH, Kanis JA, Malluche H, Meunier PJ, et al. Bone histomorphometry: Standardization of nomenclature, symbols, and units: Report of the asbmr histomorphometry nomenclature committee. J Bone Miner Res 1987;2:595–610..

[14] Whitehouse WJ. The quantitative morphology of anisotropic trabecular bone. Journal of Microscopy 1974;101:153–68..

[15] Harrigan TP, Mann RW. Characterization of microstructural anisotropy in orthotropic materials using a second rank tensor. J Mater Sci 1984;19:761–7.

[16] Cowin SC. The relationship between the elasticity tensor and the fabric tensor. Mechanics of Materials 1985;4:137–47.

[17] Musy SN, Maquer G, Panyasantisuk J, Wandel J, Zysset PK. Not only stiffness, but also yield strength of the trabecular structure determined by non-linear μFE is best predicted by bone volume fraction and fabric tensor. Journal of the Mechanical Behavior of Biomedical Materials 2017;65:808–13.

[18] Hazrati Marangalou J, Ito K, van Rietbergen B. A novel approach to estimate trabecular bone anisotropy from stress tensors. Biomech Model Mechanobiol 2015;14:39–48.

[19] Becker J, Mermoz E, Linares J-M. Joint Loading Estimation Method for Horse Forelimb High Jerk Locomotion: Jumping. J Bionic Eng 2019;16:674–85.

[20] Heyland M, Trepczynski A, Duda GN, Zehn M, Schaser K-D, Märdian S. Selecting boundary conditions in physiological strain analysis of the femur: Balanced loads, inertia relief method and follower load. Medical Engineering & Physics 2015;37:1180–5.

[21] Turner CH. On Wolff's law of trabecular architecture. Journal of Biomechanics 1992;25:1–9.

[22] Moreno R, Borga M, Smedby Ö. Techniques for Computing Fabric Tensors: A Review. In: Westin C-F, Vilanova A, Burgeth B, editors. Visualization and Processing of Tensors and Higher Order Descriptors for Multi-Valued Data, Berlin, Heidelberg: Springer; 2014, p. 271–92.

[23] Domander R, Felder AA, Doube M. BoneJ2 - refactoring established research software. Wellcome Open Res 2021;6:37.

[24] FreeCAD. 2022.